DOI: 10.31276/VJSTE.66(2).114-120

GPR investigation of the cause of persistent failure of a university road

Muslim Babatunde Aminu*, Femi Ologunaye

Department of Earth Sciences, Adekunle Ajasin University Akungba-Akoko, Akungba Akoko Town, Ondo State, Nigeria

Received 6 January 2024; revised 12 March 2024; accepted 21 March 2024

Abstract:

We present the results of a multi-frequency ground-penetrating radar (GPR) survey over a university road in south-western Nigeria that has experienced persistent failures. The goal was to evaluate causes of failure to aid remediation efforts. Data was collected concurrently at 250, 500, and 1000 MHz using a UTSI electronic trivue system. Data were processed and interpreted using Reflex-Win. Visual observations of major features apparent on the road surface including failed sections were noted. Imaged features included possible bases of the surface course, base course and sub-base, subsurface projections of an outcropping and buried basement rocks, three deeply cut and back-filled sections that lie beneath sections of the road that have experienced persistent failure, and the ringing effects and rebar-associated reflection hyperbolae of two reinforced concrete drains. Indications of preferential wetting of the shallow subsurface beneath much of the failed sections suggest that failure is due to excessive moisture content in these sections. These failed sections generally correspond to regions of deep cut and backfill, and regions cut and filled for the construction of reinforced concrete drains. Apparently, the backfills at these locations have failed to prevent water influx into the subsurface and more effective remediation measures need to be deployed.

Keywords: **ground-penetrating radar, moisture content, road failure, shallow basement.**

Classification number: **4.3**

1. Introduction

GPR is a nondestructive testing (NDT) technology device that has found applications in various fields of civil engineering, agricultural studies, archaeology, and environmental studies around the world. Electromagnetic waves of various frequency band ranges are radiated into the ground by the transmitters and the reflections are recorded by receivers. The acquired signals enable the determination of the location and disposition of the subsurface anomalies [1]. GPR applications in geotechnical investigation and engineering projects include the evaluation of the ground structure around tunnels and linings [2, 3], foundation assessment and identification of foundation strata [4, 5], location and identification of underground utilities [6, 7], inspection of road pavements [8, 9], railway subgrade and ballast characterization [10, 11], bridge deck condition assessments [12, 13], and more.

In the assessment of pavement layers for road monitoring and remediation, GPR has been applied in the detection of construction changes [14], the location of voids and sinkholes [15, 16], the identification of wet patches (indicating poor support), locating reinforcing bars [1] and mapping excess sub-base moisture [17, 18].

Many highways and roads use a bituminous binding material to make a solid, bound upper-pavement layer. Usually, the upper-pavement layer will itself consist of several individual layers of slightly varying materials. The essence is to achieve a section that provides good load distribution, prevents water ingress, and ensures a smooth ride for vehicles [14]. The basic sections of the pavement include a sub-base, a base course and a surface course (Fig. 1). The sub-base is the layer of aggregate material laid on the subgrade (*in situ* soil). The materials used may be either unbound granular, or cement-bound. It is often the main load-bearing layer of the pavement [19]. The base course is a layer usually of loosely-bound aggregates placed on the sub-base that acts to distribute traffic loads to the underlying sub-base and subgrade layers, facilitate drainage, as well as provide support to the wearing surface (surface course) to prevent tensile fatigue or cracking [20]. The surface course is the wearing course or friction course. In rigid pavements, the road consists of a concrete slab made of Portland cement while in flexible pavements, it an asphalt concrete, made up of a construction aggregate and a bituminous binder [21]. Since these components (surface bituminous course, base course, sub-base and subgrade [soil]) usually have differing dielectric constants [14], this leads to varying levels of reflection of energy emanating due to variations in the materials within the pavement structure and the subgrade beneath.

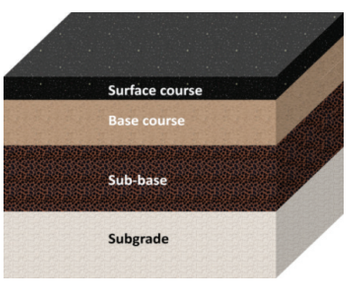

Fig. 1. Basic flexible pavement structure.

W. Xue, et al. (2023) [22] developed a back-propagated neural network algorithm for automatic detection of underground targets beneath urban roads from GPR data. The procedure involved clutter

*Corresponding author: Email: muslimaminu@gmail.com

suppression via robust principal component analysis, target domain statistical analyses, neural network recognition of target's horizontal domain and a fusion and delete (FAD) algorithm to optimize the definition of the horizontal target domains. In experimental trials, the algorithm allowed the detection of targets at a higher accuracy rate and in less time compared to two traditional segmentation recognition methods.

J.Y. Rhee, et al. (2021) [1] addressed the applications and the limitations of the GPR in the investigation and monitoring of the subsurface beneath Korean highways with a view to improving the efficient application of GPR technology. They study the depth of investigation and detection performance of anomalous objects of two different multichannel GPR systems on the Korean Expressway Corporation's nondestructive testing test-bed for subsurface detection. The results showed that the combination of the plan view by depth and cross- and longitudinal sections of the GPR data achieved from multichannel 3D GPR made analysis easier and more accurate.

S. Colagrande, et al. (2011) [23] conducted GPR investigations to study degraded road pavements built in a cut-and-fill section. They assess road integrity via quantitative analysis of power curves on GPR data collected at 1600 and 600 MHz. Comparison between the absorption coefficients of damaged and undamaged road sections allowed the determination of the cause of road degradation. Degradation was linked to fatigue and thermal shrinkage of road pavement material when the absorption angles were similar but were adduced to differential compaction of the subgrade if absorption angles were significantly dissimilar.

M.S. Abdullah, et al. (2022) [24] conducted a GPR survey at a municipal pumping station to estimate the type of soil causing differential settlement of the ground beneath the station. The study involved two surveys, involving a 160 and 450 MHz antenna, run once before and once after the injection of cement slurry into the subsurface for ground improvement. The results showed soil creep in some sections of the soil beneath the facility's foundation. Further, they effectively determined the thickness of the raft foundation beneath the structure.

J. Ling, et al. (2022) [25] developed a road subgrade monitoring method based on time-lapse full-coverage 3D GPR surveying. The focus was solving key problems related to time and spatial position mismatches in experimental data. The study used the time zero consistency correction, 3D data combination, and spatial position matching methods, which greatly improved the 3D imaging quality of underground spaces. Time-lapse attribute analysis was further used to obtain detailed characteristics and an overall pattern of the dynamic subgrade change.

T. Thitimakorn, et al. (2016) [26] used the GPR technique to investigate the potential presence of subsurface voids under the road surface in the Bangkok metropolitan area. The GPR data were collected with a 400 MHz antenna mounted on a survey cart. Several void-like anomalies were detected from the GPR data and later drilled to confirm the existence of the voids. Some GPR anomalies were found not to be voids but came from areas of past road maintenance or manholes with a hidden cover (asphalt concrete overlay).

These studies demonstrate the versatility of the GPR technique in road monitoring and maintenance. The goal of the current study was to investigate the sources of multiple recurrent failure indices on a major university road. Although the road surface had been remediated on multiple occasions, such remediations have not achieved the desired result and have not arrested the failure.

2. Ground-penetrating radar principle

The GPR technique involves transmitting high-frequency electromagnetic pulses (radar) from a transmitting antenna (or an array of antennas) into the subsurface and recording the time taken for reflected energy to return to a receiver antenna. The passage of radar waves through a material is dependent on the material type, condition, water content and pore fluid content. These properties impact the dielectric constant of the material, which in turn determines the speed of the radar pulse through the material. If two materials have sufficiently contrasting dielectric properties, some radar energy is reflected to the surface from the material boundary (Fig. 2).

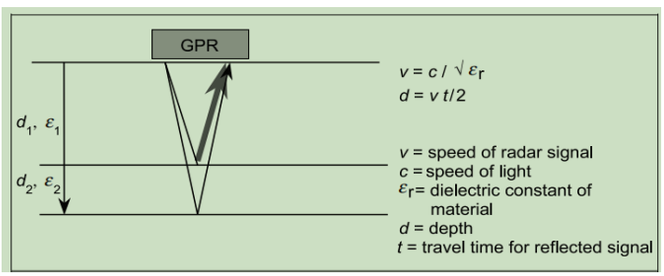

Fig. 2. Schematic of GPR technique indicting the calculation of radar pulse speed and depth [14].

GPR systems use a wide range of frequencies, usually, 100 to 2000 MHz. Higher frequencies (≥400 MHz) provide higher resolution in the shallow sections of the material but a much-limited penetration depth. This encourages their use for detailed near-surface surveys such as pavement monitoring and mapping reinforced concrete rebar conditions. Conversely, lower frequencies (≤400 MHz) provide greater depths of investigation but lower resolution capacity. They therefore find much use in geological mapping and deep archaeological studies.

3. Site of investigation

Adekunle Ajasin University is located in Akungba-Akoko in the north-eastern region of Ondo State, south-western Nigeria (Fig. 3A). Akungba-Akoko is located between 05˚43'E and 05˚47'E, and 07˚27'N and 07˚31'N. The township bounds consist of a gently sloping central low-lying region surrounded in a perimeter-like pattern by high-rising granitic hills to the north, west, east, and southeast. Topographic relief is generally beyond 345 m above sea level. Surrounding perimeters hills could rise to 420 m above sea level. The local lithology suite includes rocks of the migmatite-gneiss complex of the basement rocks characteristic of the southwestern regions of Nigeria [27]. The suite of rocks consists of biotite-rich grey gneiss, granite gneiss and lesser amounts of charnockitic rock. The area is drained by seasonal streams that start from the high reliefs in the northeastern region of the area. Regolith development

in the area is generally thin. This is appreciated from visual reconnaissance evaluation of the area; basement rocks frequently outcrop in several parts of the area. The rocks of the Akungba-Akoko area have undergone at least two episodes of tectonic deformation characteristic of the Precambrian basement complex rock of south-western Nigeria. This has engendered the development of a series of fractures and complex minor folds. Drainage courses are generally controlled by persistent major fracture systems. The survey site is a section of a major road spanning 370 m in the western campus of Adekunle Ajasin University (Fig. 3A). This university road has multiple failed sections that have been the focus of repeated and perennial remediation efforts (Fig. 3B).

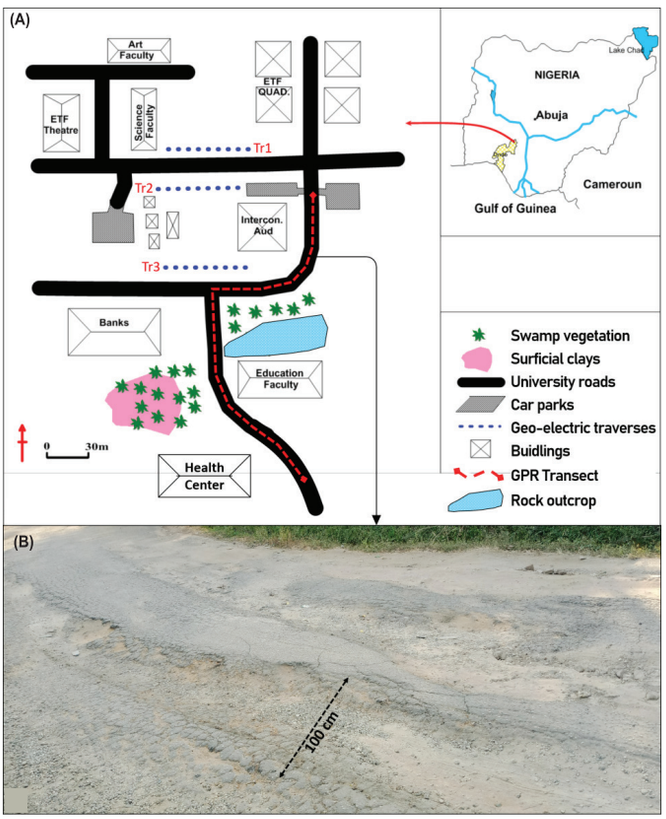

Fig. 3. Survey location. (A) GPR transect, red dashed line, traverses northwards, and takes a right turn eastwards before continuing northwards (Modified after [28]); **(B)** Failed section.

4. Methodology

A GPR transect was surveyed in this study. The transect starts from the proximate front of the University Health Centre, travels northwards and then takes an eastward turn around the south-eastern flanks of the Intercontinental Bank Auditorium before terminating north a few meters before a four-way junction (Fig. 3). The transect length was 370 m. GPR data was collected using a triple-frequency UTSI Electronic Trivue system with bandwidths of 125-500, 200-800, and 500-2000 MHz centred on 250, 500 and 1000 MHz, respectively. The antennas are co-centred. Record times were 80, 60, and 40 ns for the 250, 500, and 1000 MHz records, respectively. Triggering was via an encoder wheel system which also records the length of the transects. Data was collected in the month of October (2023) towards the end of the rainy season. Visual observations of key features along the road were made and documented. These included failed road portions, speed bumps, reinforced concrete drains, and outcropping basement rocks (Table 1). Data processing was accomplished in Reflex-Win version 10.1 and followed a sequence including (Table 2, Fig. 4): (1) Dewow, (2) Static correction, (3) Gain, and (4) Background removal. The outputs were 2D GPR radar-grams plotted in time (ns) versus lateral position. The final sections are presented in grayscale as this provides the best opportunity to identify features.

Table 1. Features noted along the GPR transect.

No.	Feature	Position (m)
1	Start of transect	0
2	Failed section 1- (concrete mend)	7-20 (7-20)
3	Speed bump 1	12
4	Failed section 2	48-59
5	Reinforced concrete drain	63-65
6	Failed section 3	108-162
7	Outcropping basement rock	145-161
8	The first turn starts (right)	208
9	Failed section 4	210-212
10	Reinforced concrete drain	210-211
11	Failed section 5	232-242
12	The second turn starts (left)	268
13	Failed section 6 (concrete mend)	273-342 (311-330)
14	Speed bump 1	340
15	End of transect	370

Table 2. GPR processing sequence.

No.	Processing sequence ID	Parameter		
		250 MHz	*500 MHz*	*1000 MHz*
1	Dewow	64 ns	32 ns	16 ns
2	Static correction	Variable	Variable	Variable
3	Gain (exponential)	0.5	1	2
4	Background removal	Automatic	Automatic	Automatic

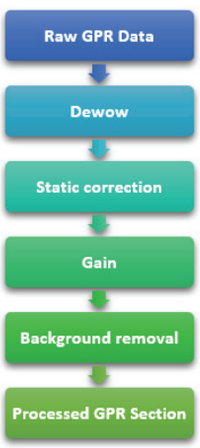

Fig. 4. Workflow sequence used for processing the GPR data.

5. Results

Only the 500 and 1000 MHz sections are presented in this study (Figs. 5-8). These sufficiently highlight the various features identified in the study area and enable ample interpretation. The 250 MHz sections were of very low resolutions for most features and as the area is generally of thin overburden thickness, no significant features were imaged at the greater depths it provided. Generally, the 1000 MHz section provided higher resolutions and more detailed imaging of the very shallow subsurface (0-8 ns) and allowed a better interpretation of features in the very shallow subsurface compared to the 500 MHz section. Conversely, the 500 MHz allowed better imaging and interpretation of major features at depth and allowed the identification of further extensions of features not completely imaged on the 1000 MHz section.

Persistent reflections are identified at 0.5, 1.5, and 4 ns, respectively on the 1000 MHz section. They however appear lumped together and indistinct in the 500 MHz section. These reflections are generally continuous all through the transect except at failed portions of the road, specifically at 7-20, 48-49, 108-162, 232-242, and 273-342 m. At these locations, the reflections become discontinuous and have much lower reflection amplitudes and lower reflection cycles. They may also present as undulating reflections, or as hyperbola-interrupted reflections. These undulations are particularly apparent at 90-110, and 130-145 m at average depths of 2-4 ns two-way time (twt). Speed bump locations present with concave upwards reflections at 10-11 and 341-342 m with ringing effects that persist with depth (Figs. 5 and 8). The known concrete drains present strong elevated platform-like amplitude reflections at 62-65 and 209-211 m (Figs. 5 and 7). On either side of the drain at 62-65 m, reflections show a sag at 4 ns that extends to about 12 ns twt. The drain reflections also show a ringing effect continuous at depth. In the 500 MHz sections, multiple tightly packed and overlapping hyperbolae are visible. Slight variations occur between the noted locations of the speed bumps and concrete drain (Table 1) and their reflected locations on the GPR transect.

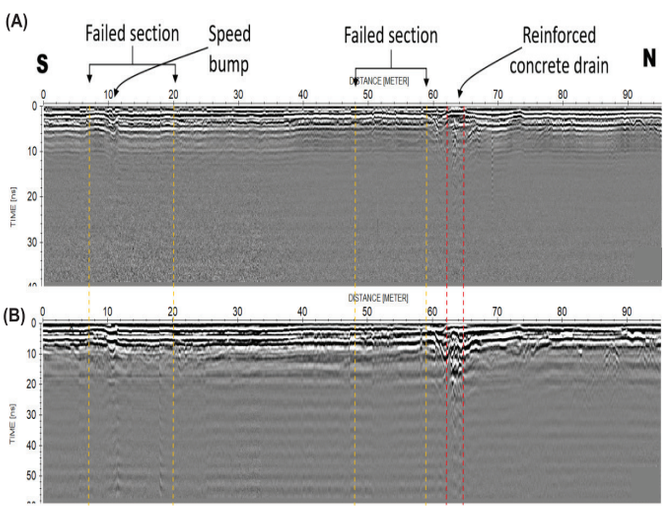

Fig. 5. 0-90 m GPR composite image of processed (A) 1000 MHz, (B) 500 MHz section. Failed road sections, a speed bump and a reinforced concrete drain are indicated at 7-20, 48-59, 11, and 62-53 m, respectively along the transect.

At 132-155 m, strong amplitude reflections occur in the first 4 ns twt (Fig. 6). Beneath this region, steeply dipping strong amplitude reflections coincide with the lateral position of a rock mass outcropping to the east of the Transect. The reflections are continuous, strongly undulating and the southwards dipping arm extends beyond 40 ns twt in the 500 MHz section. The northward arm appears to dip at greater angles but is only imaged to less than 30 ns twt.

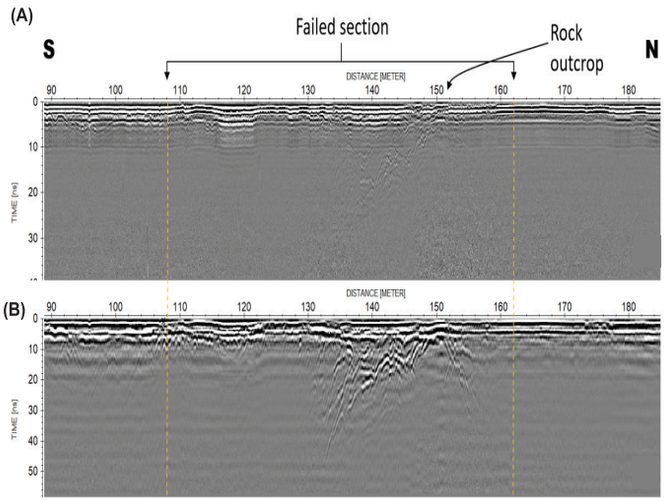

Fig. 6. 90-180 m GPR composite image of processed of (A) 1000 MHz, (B) 500 MHz section. The failed road section spans 108-162 m. Lateral amplitude loss is noted at 90-116 m, and 122-136 m in the shallow (<8 ns) section of the 1000 MHz image. Strong amplitude dipping reflections occur beneath the location of the outcropping rock noted at 145-161 m and extend to over 45 ns.

Significant lateral loss of reflection amplitudes within the upper 8 ns of the 1000 MHz section occurs at 72-82, 90-116, 122-136, 213-217, 232-260, and 278-311 m (Figs. 5-8). At these locations, the reflection amplitude is much dimmer than in adjacent locations. In the 500 MHz, these locations may display little amplitude loss. They, however, frequently present as more discontinuous reflections relative to adjacent locations. At 215-228 m, a second dipping strong amplitude reflection is well imaged on the 500 MHz section (Fig. 7). This reflection is not imaged on the 1000 MHz section. At its upper end, it borders the location of the reinforced concrete drain at 209-211 in a zone characterised by chaotic reflections. This zone presents with significant amplitude loss in the 1000 MHz section.

Three regions of relatively chaotic low amplitude reflections are identified at depths beyond the 10 ns mark on the 500 MHz sections (Figs. 7 and 8). These regions occur at 225-250, 275-305, and 317-343 m. These regions extend up to 25, 37, and 26 ns, respectively. The bottom of the 225-250 region is a smooth basin-like structure but the bottoms of the 275-305 and 317-343 m regions present as undulating bases. Within these basin-like sections, the reflection character differs considerably and is more chaotic relative to adjacent sections. At 311-330 m, a concrete overlay has been applied to the failed road (Fig. 8). In shallow (<5 ns) sections beneath the concrete overlay, strong amplitude and continuous reflection akin to the shallow continuous reflection earlier noted at 0.5, 1.5, and 4 ns are observed. However, in-between the reflections, the reflection character is chaotic.

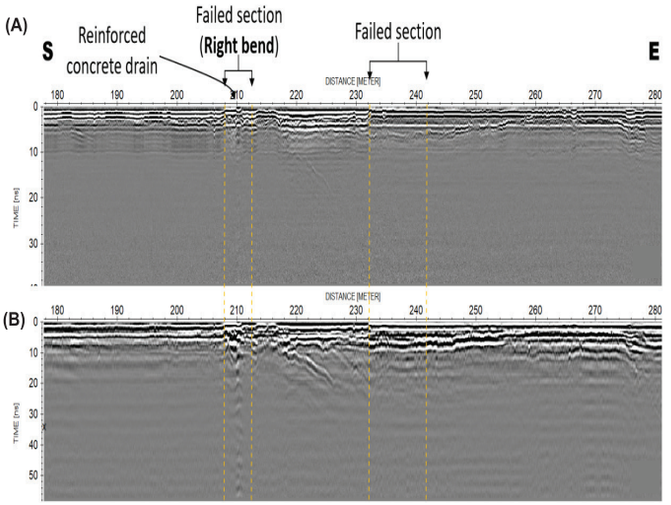

Fig. 7. 180-280 m GPR composite image of processed of (A) 1000 MHz, (B) 500 MHz section. Failed road sections span 208-212 m and 232-242 m. Lateral amplitude loss is noted at 213-217 and 232-260 m in the shallow (<8 ns) section of the 1000 MHz image. A second strongly dipping set of high-amplitude reflections is imaged at 215-228 m on the 500 MHz image. At 225-250 m, significantly disturbed reflections are observed beyond 10 ns.

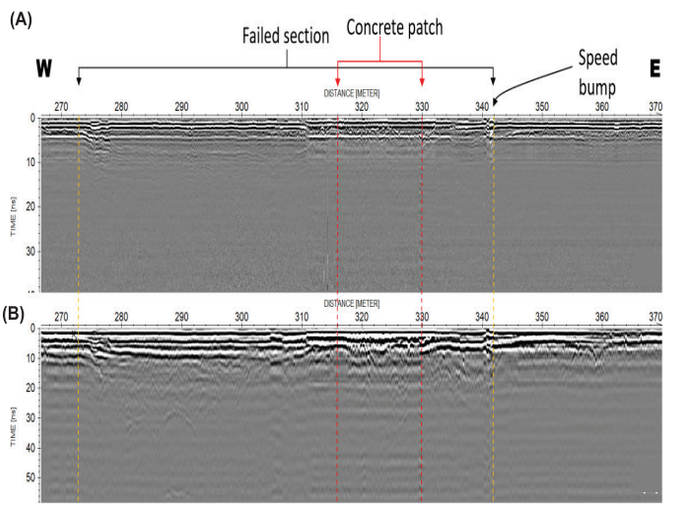

Fig. 8. 270-370 m GPR composite image of processed of (A) 1000 MHz, (B) 500 MHz section. The failed road section spans 273-342 m. A concrete patch has been applied to 316-330 m. At 275-305 and 317-343 m, significantly disturbed reflections which form bowl-shaped morphologies extend to depths beyond 25 ns.

6. Discussion

Figure 9 represents a cartoon of our interpretation of the GPR transect along the road. Previously, a geo-electric traverse was surveyed close to a section of the transect in this study. Details of the survey and interpretation can be found in [28]. The locations of the geo-electric traverses are indicated in Fig. 3.

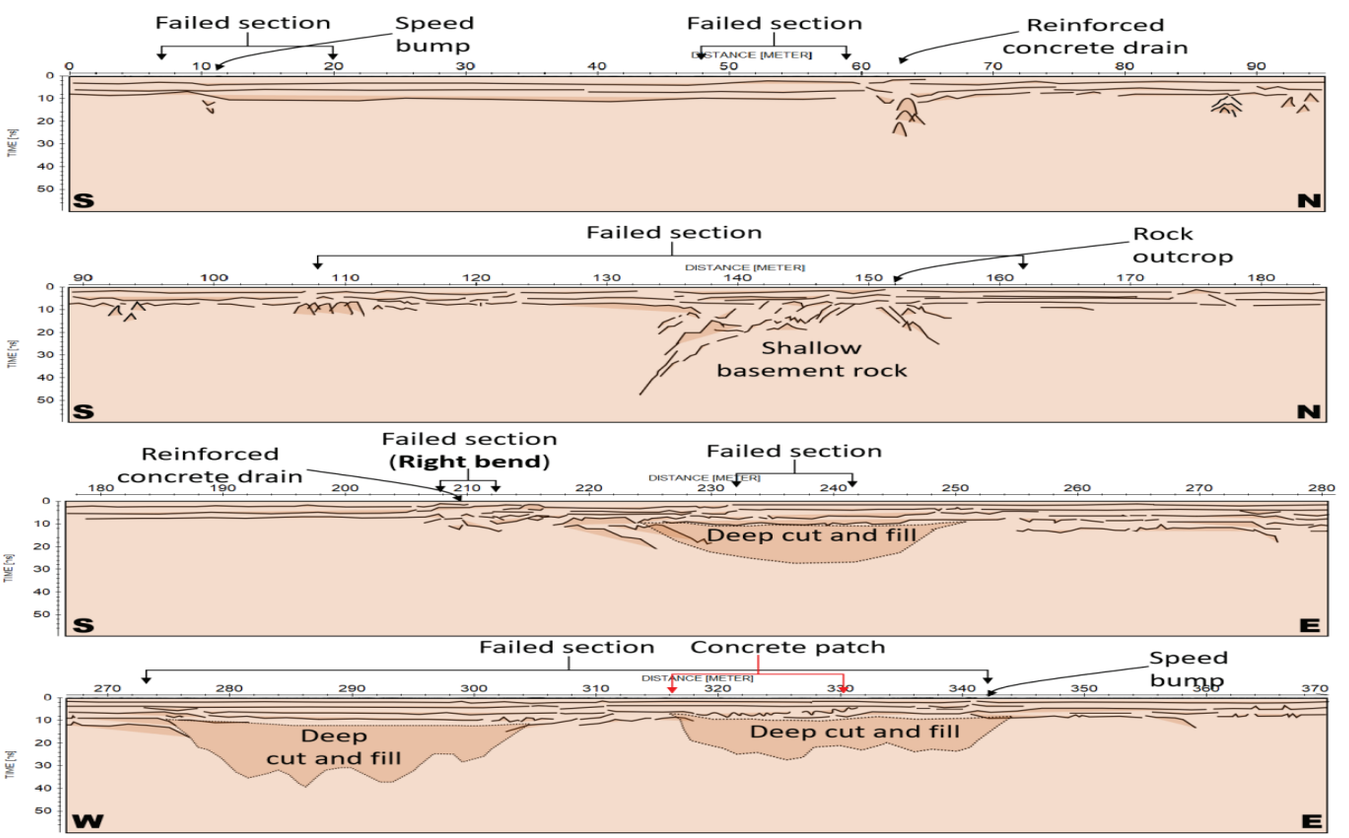

Fig. 9. Interpretation carton of the subsurface along the road transect. Road failure is associated with regions with very shallow-to-outcropping bedrock at 215-228 and 145-161 m, respectively, and deeply back-filled sections at 275-305 and 317-343 m.

Based on a transmission velocity of 0.1 m/ns that has been recommended for subsurface materials beneath tarmac [29], the continuous reflections identified at 0.5, 1.5, and 4 ns twt, on the 1000 MHz section correspond to depths 0.025, 0.075, and 0.2 m, respectively. These reflections may correspond to the base of the surface course, the base of the base course, and the base of the sub-base along the road, respectively. We do not have independent confirmation of these interpretations but these values represent typical values of surface course, base course and sub-base course in the area. These reflections become way more chaotic toward the second half of the transect (>210 m). The presence of ringing at depth beneath the reinforced concrete drains is due to the air gap between the drains' upper slab and its floor [29]. Tightly packed hyperbolae at the drain (62-65 m) likely represent reflections from individual rebars in the upper slab reinforcement of the drain. We interpret the reflection sags observed on either side of the drain as evidence of previous excavation and backfill during the construction of the drain. Differential compaction between the original subgrade and fill material may have preserved the line of cut and given rise to the apparent sag.

We further interpret the lateral amplitude losses along reflections at 72-82, 90-116, 122-136, 213-217, 232-260, and 278-311 m as related to elevated water content at these locations [14, 29, 30]. The presence of water in the near-surface slows the GPR wave and broadens it in the time direction. We interpret the three chaotic regions at 225-250, 275-305, and 317-343 m to represent areas of considerably thicker overburden relative to the rest of the transect. These regions likely represent regions of deeply excavated and back-filled overburden. They align considerably well with failed sections of the road at 210-212, 232-242, and 273-342 m.

We contend that failure along the road is primarily due to the presence of excess amounts of water in the subsurface at the failed sections. The outcropping rock mass at 132-155 m likely sheds much precipitation runoff during the rains into the shallow subsurface at the failed section at 108-162 m. The second dipping high amplitude reflection at 215-228 m likely represents the presence of a second near-surface rock mass at this location. Only one arm (east dipping) of the rock mass is indicated as the other arm (likely west dipping) lies west of the first turn (and is beyond the coverage) of the GPR transect. It is worth noting that [28] imaged a neck-like weathering-resistant shallow basement over which the university road passes at this junction (Fig. 10).

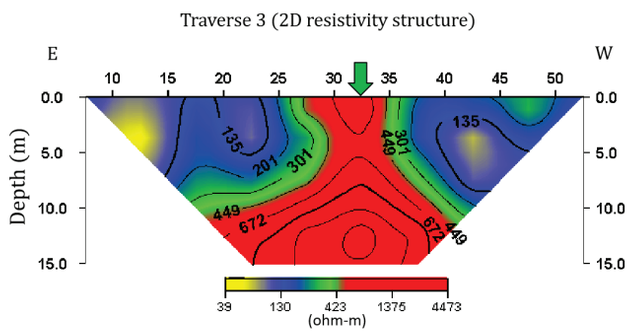

Fig. 10. 2D subsurface resistivity structure along the southernmost geo-electric traverse (Tr 3) which runs adjacent to part of the GPR transect [28] (see Fig. 3 for spatial relationship with the GPR transect).

Outcrops of this rock can be seen much further west, north of the Banks' location. The chaotic regions imaged at depth (extending >10 ns) lie in regions coincident with a clayey aquitard imaged in [28] (Fig. 10). This clayey aquitard extends to depths in excess of 10 m in the eastern bend of the current transect. The bowl-shaped chaotic regions appear to lie within a region that is a lateral equivalent to this clayey aquitard and may represent deep excavations and backfill of the clayey aquitard along the road. The chaotic internal reflections here likely represent coarser rock fill intended to stabilise the subsurface beneath this section of the road. Apparently, the excavation and fill have not been sufficiently effective to prevent water from saturating the near-surface materials along the sections of the road. This is where the road fails extensively, and even though a section of it has been remediated with a concrete overlay, the road still experiences much damage. The basement arm imaged at 215-228 possibly also sheds much runoff eastwards into this cut and fill section encouraging its wetness and attendant instability.

7. Conclusions

We have presented the results of a GPR survey aimed at determining the causes of multiple failures of a road that have defied repeated remediation courses. The major factors causing the failures, in our opinion, are related to deeply excavated and back-filled regions and regions cut and filled for the construction of reinforced concrete drainage. Though the deeply excavated regions were meant to remediate a section initially filled with a clayey aquitard, they have failed to prevent the ingress of groundwater which saturates the shallow subsurface at these locations and leads to much instability at the surface. A further contribution to the saturation of the shallow subsurface at failed locations likely comes from their proximity to shallow basement rocks that serve to shed precipitation runoff toward these sections. The result of the survey allowed a re-construction of the shallow subsurface along the road and the identification of the major causes of recurrent failure. It is hoped this would help in the design of effective remediation measures to prevent future failure.

CRediT author statement

Muslim Babatunde Aminu: Conceptualisation and Methodology, Writing - Original draft preparation; Femi Ologunaye: Methodology and Editing.

ACKNOWLEDGEMENTS

We are grateful to the Agrosoil Research Team at Adekunle Ajasin University for providing access to the trivue GPR system and the Reflexw-10 software used in this study.

COMPETING INTERESTS

The authors declare that there is no conflict of interest regarding the publication of this article.

REFERENCES

[1] J.Y. Rhee, K.T. Park, J.W. Cho, et al. (2021), "A study of the application and the limitations of GPR investigation on underground survey of the Korean expressways", *Remote Sensing*, **13(9)**, DOI: 10.3390/rs13091805.

[2] J.L. Porsani, Y.B. Ruy, F.P. Ramos, et al. (2012), "GPR applied to mapping utilities along the route of the line 4 (yellow) subway tunnel construction in São Paulo City, Brazil", *Journal of Applied Geophysics*, **80**, pp.25-31, DOI: 10.1016/j.jappgeo.2012.01.001.

[3] National Academies of Sciences, Engineering, and Medicine (2013), *Mapping Voids, Debonding, Delaminations, Moisture, and Other Defects Behind or Within Tunnel Linings*, The National Academies Press, 32pp, DOI: 10.17226/22609.

[4] V.R. Balasubramaniam, P.C. Jha (2010), "Imaging for foundation defects using GPR", *Proceedings of The 13th International Conference on Ground Penetrating Radar*, pp.1-5, DOI: 10.1109/ICGPR.2010.5550201.

[5] V.V. Pupatenko, Y.A. Sukhobok, G.M. Stoyanovich (2017), "Lithological profiling of rocky slopes using georeader software based on the results of ground penetrating radar method", *Procedia Engineering*, **189**, pp.643-649, DOI: 10.1016/j.proeng.2017.05.102.

[6] S.H. Ni, Y.H. Huang, K.F. Lo, et al. (2010), "Buried pipe detection by ground penetrating radar using the discrete wavelet transform", *Computers and Geotechnics*, **37(4)**, pp.440-448, DOI: 10.1016/j.compgeo.2010.01.003.

[7] K.K.K. Singh, I. Kumar, U.K. Singh (2013), "Interpretation of voids or buried pipes using ground penetrating radar modeling", *Journal of The Geological Society of India*, **81**, pp.397-404, DOI: 10.1007/s12594-013-0050-6.

[8] P. Shangguan, I.A. Qadi, A. Coenen, et al. (2016), "Algorithm development for the application of ground-penetrating radar on asphalt pavement compaction monitoring", *International Journal of Pavement Engineering*, **17(3)**, pp.189-200, DOI: 10.1080/10298436.2014.973027.

[9] S. Zhao, I.L.A. Qadi (2016), "Development of an analytic approach utilizing the extended common midpoint method to estimate asphalt pavement thickness with 3-D ground-penetrating radar", *NDT & E. International*, **78**, pp.29-36, DOI: 10.1016/j.ndteint.2015.11.005.

[10] J. Hugenschmidt (2000), "Railway track inspection using GPR", *Journal of Applied Geophysics*, **43(2-4)**, pp.147-155, DOI: 10.1016/S0926-9851(99)00054-3.

[11] F. Tosti, B.L. Ciampoli, A. Calvi, et al. (2018), "An investigation into the railway ballast dielectric properties using different GPR antennas and frequency systems", *NDT & E International*, **93**, pp.131-140, DOI: 10.1016/j.ndteint.2017.10.003.

[12] K. Dinh, N. Gucunski, J. Kim, et al. (2015), "Attenuation-based methodology for condition assessment of concrete bridge decks using GPR", *Proceedings of The 32nd International Symposium on Automation and Robotics in Construction and Mining: Connected to The Future, Proceedings, Oulu, Finland, 15-18 June 2015*, DOI: 10.22260/ISARC2015/0055.

[13] J.Y. Rhee, J.J. Choi, S.H. Kee (2019), "Evaluation of the depth of deteriorations in concrete bridge decks with asphalt overlays using air-coupled GPR: A case study from a pilot bridge on Korean expressway", *International Journal of Concrete Structures and Materials*, **13**, pp.1-17, DOI: 10.1186/s40069-018-0327-7.

[14] R. Evans, M. Frost, M.S. Jones, et al. (2006), "Ground-penetrating radar investigations for urban roads", *Proceedings of The Institution of Civil Engineers Municipal Engineer*, **159(ME2)**, pp.105-111, DOI: 10.1680/muen.2006.159.2.105.

[15] J. Sevil, F. Gutiérrez, M. Zarroca, et al. (2017), "Sinkhole investigation in an urban area by trenching in combination with GPR, ERT and high-precision leveling. Mantled evaporite karst of Zaragoza city, NE Spain", *Engineering Geology*, **231**, pp.9-20, DOI: 10.1016/j.enggeo.2017.10.009.

[16] J. Baek, J.S. Yoon, C.M. Lee, et al. (2018), "A case study on detection of subsurface cavities of urban roads using ground-coupled GPR", *Proceedings of The 17th International Conference on Ground Penetrating Radar, Rapperswil, Switzerland*, DOI: 10.1109/ICGPR.2018.8441653.

[17] R.C. Schwartz, S.R. Evett, M.G. Pelletier, et al. (2009), "Complex permittivity model for time domain reflectometry soil water content sensing: I. Theory", *Soil Science Society of America Journal*, **73(3)**, pp.886-897, DOI: 10.2136/sssaj2008.0194.

[18] M.R.M. Ardekani (2013), "Off- and on-ground GPR techniques for field-scale soil moisture mapping", *Geoderma*, **200-201**, pp.55-66, DOI: 10.1016/j.geoderma.2013.02.010.

[19] M.Y. Fattah, M.M. Hilal, H.B. Flyeh, et al. (2016), "Effect of fine material on compaction characteristics of subbase material using the Superpave gyratory compactor", *International Journal of Civil Engineering and Technology*, **7(5)**, pp.466-476.

[20] H.H. Titi, H. Tabatabai, J. Ramirez, et al. (2019), *Evaluation of Recycled Base Aggregates*, Report No. 0092-17-01, Wisconsin Highway Research Program Technical Report.

[21] P. Bolander, V. Barandino, G. Keller (2022), "Guidelines for road surface course aggregate", *National Technology and Development Program*, *Technical Report 2277-1804-NTDP 7700-Transportation Management.*

[22] W. Xue, K. Chen, T. Li, et al. (2023), "Efficient underground target detection of urban roads in ground-penetrating radar images based on neural networks", *Remote Sensing*, **15(5)**, DOI: 10.3390/rs15051346.

[23] S. Colagrande, D. Ranalli, M. Tallini (2011), "Ground penetrating radar assessment of flexible road pavement degradation", *International Journal of Geophysics*, **2011**, DOI: 10.1155/2011/989136.

[24] M.S. Abdullah, H.H. Karim, Z.W. Samueel (2022), "Investigation structural settlement by ground penetrating radar (Case study)", *IOP Conference Series: Earth and Environmental Science*, **961**, DOI: 10.1088/1755-1315/961/1/012037.

[25] J. Ling, R. Qian, K. Shang, et al. (2022), "Research on the dynamic monitoring technology of road subgrades with time-lapse full-coverage 3D ground penetrating radar (GPR)", *Remote Sensing*, **14(7)**, DOI: 10.3390/rs14071593.

[26] T. Thitimakorn, N. Kampananon, N. Jongjaiwanichkit, et al. (2016), "Subsurface void detection under the road surface using ground penetrating radar (GPR), a case study in the Bangkok metropolitan area, Thailand", *International Journal of Geo-Engineering*, **7**, DOI: 10.1186/s40703-016-0017-8.

[27] A.C. Ogunyele, O.A. Oluwajana, I.Q. Ehinola, et al. (2019), "Petrochemistry and petrogenesis of the Precambrian basement complex rocks around Akungba-Akoko, southwestern Nigeria", *Material and Geoenvironment*, **66(3)**, pp.173-183, DOI: 10.2478/rmzmag-2019-0036.

[28] M.B. Aminu (2015), "Electrical resistivity imaging of a thin clayey aquitard developed on basement rocks in parts of Adekunle Ajasin University campus, Akungba-Akoko, south-western Nigeria", *Environmental Research Engineering and Management*, **71(1)**, pp.47-55, DOI: 10.5755/j01.erem.71.1.9016.

[29] E.C. Utsi (2017), *Ground Penetrating Radar: Theory and Practice*, Butterworth - Heinemann, 224pp.

[30] N.N. Halimshah, A. Yusup, Z.M. Amin, et al. (2015), "Visual inspection of water leakage from ground penetrating radar radargram", *Remote Sensing and Spatial Information Sciences*, pp.191-198, DOI: 10.5194/isprsannals-II-2-W2-191-2015.